8th International OpenFOAM® Workshop
June 11- 14, 2013
Jeju, Korea

Development and validation of a local time stepping-based PaSR solver for combustion and radiation modeling

Kar Mun Pang[*, ‡], Anders Ivarsson, Sajjad Haider, Jesper Schramm

Department of Mechanical Engineering, Technical University of Denmark
Nils Koppels Allé, 2800 Kgs. Lyngby, Denmark

Abstract

In the current work, a local time stepping (LTS) solver for the modeling of combustion, radiative heat transfer and soot formation is developed and validated. This is achieved using an open source computational fluid dynamics code, OpenFOAM. Akin to the solver provided in default assembly i.e. *reactingFoam*, the solver developed here is also applicable for reacting flows but it utilizes the LTS approach which assists in reducing the computational runtime. Magnussen soot model is also incorporated into the code to simulate soot formation process. Besides this, the Weighted Sum of Gray Gases Model library in the *edcSimpleFoam* solver which was introduced during the 6th OpenFOAM workshop is modified and coupled with the current solver. One of the main amendments made is the integration of soot radiation submodel since this is significant in rich flames where soot particles are formed. The new solver is henceforth addressed as *radiationReactingLTSFoam* (*rareLTSFoam*). A performance benchmarking exercise is here carried out to evaluate the effect of each LTS parameter on calculation stability, results accuracy and computational runtime. The model validation uses two test cases. The first test case presents the modeling of a helium-stabilized, laminar premixed flame at rich condition in which soot formation is observed. Here, the solver is validated by comparing both the computed temperature and soot volume fraction along the axial direction against experimental measurements and simulation results generated by ANSYS CFX. As compared to the computational runtime required by the counterpart transient solver, a speedup of approximately fourteen-fold is obtained. In the second case, a turbulent non-premixed flame, namely Sandia Flame D is simulated. The computed and measured axial temperatures are compared. The *rareLTSFoam* solver has been proved to predict the temperature and soot volume fraction of both the flames reasonably well.

‡ Corresponding author: Kar Mun Pang (kmpan@mek.dtu.dk)

1. INTRODUCTION

In the recent years, an open source computational fluid dynamics (CFD) code, OpenFOAM has been gaining attention. A brief review shows that various researchers have implemented or developed different reacting flow solvers on this platform for their respective flame studies. Christ [1] and Harasek et al. [2] used the Eddy Dissipation Concept (EDC) model for the turbulent combustion simulations of methane fuel. The solver was named as the *edcSimpleFoam*. Andersen and Nielsen [3] also exploited the EDC approach to numerically investigate the combustion event of a burner flow reactor. On the other hand, Kassem et al. [4] implemented the Eddy Dissipation Model to simulate a confined non-premixed methane jet flame. Apart from these, Marzouk and Huckaby [5] exploited the default reacting solver provided in the OpenFOAM assembly, *reactingFoam* to simulate the turbulent combustion of syngas. The turbulence-chemistry interaction was modeled based the Partially Stirred Reactor (PaSR) concept. Nogenmyr et al. [6] proposed a modified version of *reactingFoam* based on an assumption of low Mach (LM) number. As such, the thermodynamic and dynamic pressures are decoupled. The formulated solver was addressed as *reactingLMFoam* and was used together with Large Eddy Simulations (LES) for the modeling of a piloted lean-premixed jet flame [7]. Likewise, Duwig et al. [8] implemented *reactingLMFoam* to numerically study the flow and dynamics in a swirling combustor operated at a partially premixed condition. Besides this, Cuoci et al. [9, 10] developed the *libOpenSMOKE* code with OpenFOAM. The flamelet concept was employed for the modeling of turbulent non-premixed flame. Various soot formation submodels were also provided in their solver library. In addition, Messig et al. [11] implemented the flamelet model to examine the laminar diffusion flames. The work was carried out with *diffusionFoam*, an extension of their existing solver *alternateReactingFoam* which the latter solver is a link-up between OpenFOAM and the Cantera library [12].

1.1 Motivation of the Study

In the current work, *reactingFoam* which employs the PaSR model as the turbulence-chemistry interaction model is selected here. Nevertheless, *reactingFoam* is a transient solver and the computation runtime required for the associated reacting flow simulations could be impractical. This is particularly true here when a multi-dimensional computational domain with high mesh resolution is required at regions with high temperature and species gradients. The computational cost further escalates when detailed chemistry and comprehensive radiative transport equation such as Finite Volume Discrete Ordinate Method (fvDOM) are implemented. Apart from this, the default *reactingFoam* is not fully equipped for combusting flow simulations. The commonly used absorption/emission submodels for radiative heat transfer in combustion simulations, Weighted Sum of Gray Gas Model (WSGGM) [1, 13, 14] as well as soot formation transport equation are not implemented in the default *reactingFoam* code. Set against these backgrounds, the core objective of this work is to develop and validate a solver which has the capability to simulate combustion, radiative heat transfer and soot formation at an expedited calculation. An in-house solver which uses the local time stepping (LTS) approach is developed and its validity is assessed through comparisons with experimental data of both laminar and turbulent flames.

1.2 Structure of the Reported Work

The paper is structured such that the governing transport equations and submodels applied in the current CFD simulations are first detailed. This is then followed by the descriptions of the LTS solver. The subsequent section discusses the mesh configuration and boundary conditions of both the DTU helium-stabilized, laminar premixed flame and the Sandia Flame D. Effect of each LTS parameter on computational runtime, solution stability and results accuracy are then evaluated through a performance benchmarking study. The following section of the article reports the validation of the current model by comparing the simulated results with experimental data. In the final section of the paper, key conclusions from the work are highlighted.

2. GOVERNING EQUATIONS AND CFD MODELS

The current solver is developed by modifying an existing solver, *LTSReactingParcelFoam*. Akin to *reactingFoam* which has been widely used in combustion simulations, *LTSReactingParcelFoam* is also applicable for combusting flow but it is a LTS solver. Multiphase Lagrangian parcels and porous media are by default taken into account. In order to simplify the code, these two models which are not required are removed. In addition to this, Magnussen soot model is incorporated into the code to simulate soot formation process [15]. Besides, the Weighted Sum of Gray Gases Model (WSGGM) library in the *edcSimpleFoam* solver which was introduced by Christ [1] during the 6th OpenFOAM workshop is modified and coupled with the current solver. One of the main amendments made is the integration of soot radiation submodel since this is significant in rich flames where soot particles are formed. Modification is also made such that the partial pressures of H_2O and CO_2 (p_w and p_c) are taken into account for gas-phase radiation modeling. The modified version is henceforth addressed as *radiationReactingLTSFoam* (*rareLTSFoam*).

In a laminar flame case, the continuity, momentum and sensible enthalpy, species mass are expressed in the following partial differential equations (PDEs) form shown by Equation (1) to (4).

$$\frac{\partial \rho}{\partial t} + \nabla \cdot (\rho \vec{v}) = 0 \tag{1}$$

$$\frac{\partial \rho \vec{v}}{\partial t} + \nabla \cdot (\rho \vec{v}\vec{v}) = -\nabla p + \nabla \cdot \vec{\tau} + \rho \vec{g} \tag{2}$$

$$\frac{\partial \rho h_s}{\partial t} + \nabla \cdot (\rho \vec{v} h_s) = \nabla \cdot (\alpha \nabla h_s) + \frac{\partial p}{\partial t} + \dot{\omega}_T + \dot{q}_r \tag{3}$$

$$\frac{\partial \rho Y_i}{\partial t} + \nabla \cdot (\rho \vec{v} Y_i) = \nabla \cdot (\mu_i \nabla Y_i) + \kappa R R_i \tag{4}$$

$\dot{\omega}_T$ and $\dot{q}_r$ in Equation (3) denote the heat release due to combustion and radiative heat flux, respectively. Also, as can be seen in Equation (3), the Lewis number is by default set as unity, indicating that the heat and mass transfer are at the same rate by convection. Besides this, it is shown by Equation (4) that the Schmidt number is set as unity, indicating that the rates of momentum and mass diffusion are equivalent. The dynamic thermal diffusivity, α in Equation (3) is dependent on the thermal conductivity of the mixture which is calculated using the Eucken model. On the other hand, the dynamic viscosity, μ in Equation (4) is computed based on the Sutherland transport model. It is noteworthy that the reaction and thermophysical properties are defined using the native OpenFOAM format to specify the transport properties for each specie. Otherwise, the transport properties of O_2 specie are used for all the species if the CHEMKIN reader format is applied.

On the other hand, The last term on the right hand side of the Equation (4) represents the chemical source term. When turbulence is present, the turbulence-chemistry interaction is modeled based on the PaSR approach [16] where the reactive volume fraction, $\boldsymbol{\kappa}$ is calculated as

$$\kappa = \frac{\tau_{res} + \tau_c}{\tau_{res} + \tau_c + \tau_{mix}} \tag{5}$$

τ_{res}, τ_c and τ_{mix} represent the residence time, chemical reaction time and mixing time, respectively. If the flow is laminar and turbulent reaction does not exist, τ_{mix} is automatically set to zero, yielding a $\boldsymbol{\kappa}$ value of unity.

The radiative heat transfer study here focuses on the radiation modeling with the spherical harmonic P1 approximation to solve the radiative transport equation (RTE) [13, 14]. The P1 model

solves an advection–diffusion equation for the mean local incident radiation, G. The P1 model solves PDE in the form of

$$\nabla \cdot (\Gamma \nabla G) - aG = -(4e\sigma_{SB}T^4 + E) \quad (6)$$

where a, e and E represent the absorptivity, emissivity and emission contribution, respectively. σ_{SB} denotes the Stefan-Boltzmann constant (=5.670373 x 10^{-8} $Wm^{-2}K^{-4}$) and diffusive coefficient, Γ is calculated as follows,

$$\Gamma = \frac{1}{3(a+\sigma) - C\sigma} \quad (7)$$

where σ represents the scattering coefficient while C is a linear-anisotropic phase function coefficient. The constant scatter model is applied in the current work for the scattering process. Both values are set as zero and scattering is assumed to be isotropic [17]. The default OpenFOAM radiation absorption/emission library does not comprise WSGGM. The associated codes are hence integrated into the library. The WSGGM provides the total absorptivity and emissivity of a gas mixture as a sum of emissivities of fictitious gray gases weighted with a temperature dependent weighting factor [14, 18, 19]. The weighted emissivities, ε is then substituted into the following equation in order to calculate a and e terms introduced in Equation (6).

$$a = e = \frac{-\ln(1-\varepsilon)}{L} \quad (8)$$

where ε and L denote the emissivity and mean path length, respectively. In order to reduce the computational efforts, the absorption and emission coefficients are calculated using the same method [18]. For radiative heat transfer attributed by the gas-phase combustion products i.e. H_2O and CO_2, the weighted emissivities of a number of gray gases are dependent on the temperature as well as concentrations of both H_2O and CO_2 and vary when the p_w to p_c ratio changes. In the rich, sooty flame, soot radiation is expected to play an important role in the radiative heat transfer [20]. Here, the weighted emissivity here is dependent on both the temperature and soot concentration.

By default, no soot model is provided in the OpenFOAM library. Magnussen soot model is here coupled with the current solver to predict the associated formation process [15]. The soot concentration also serves as a necessary input for the soot radiation modeling as discussed earlier. An assumption made in the Magnussen model is that soot is formed from the gaseous fuel in two phases. The first phase denotes formation of radical nuclei while the second represents the soot particle formation from the nuclei. In the Magnussen model, two transport equations as described by Equations (9) and (10) are solved for the specific concentration of radical nuclei, X_N and the soot mass fraction, Y_S, respectively. The source terms for formation of nuclei, $S_{nuclei,f}$ and soot, $S_{soot,f}$ as well as for combustion of nuclei, $S_{nuclei,c}$ and soot, $S_{soot,c}$ are calculated using the empirical models of Tesner et al. [21].

$$\frac{\partial \rho X_N}{\partial t} + \nabla \cdot (\rho \vec{v} X_N) = \nabla \cdot (\mu \nabla X_N) + S_{nuclei,f} + S_{nuclei,c} \quad (9)$$

$$\frac{\partial \rho Y_S}{\partial t} + \nabla \cdot (\rho \vec{v} Y_S) = \nabla \cdot (\mu \nabla Y_S) + S_{soot,f} + S_{soot,c} \quad (10)$$

For the turbulence modeling in the turbulent flame case, the Reynolds-averaged Navier–Stokes (RANS) equations are applied. Due to the turbulence closure, an effective thermal diffusivity, α_{eff} and

the effective viscosity μ_{eff} are implemented [5]. Here, an additional term, turbulent viscosity, μ_t is required and is computed using Equation (11).

$$\mu_t = C_\mu \rho \frac{k^2}{\varepsilon} \tag{11}$$

where k and ε are the turbulent kinetic energy per unit mass and dissipation rate, respectively while the standard k-ε model is selected to solve these variables. The associated transport equations are as follows,

$$\frac{\partial \rho k}{\partial t} + \nabla \cdot (\rho \vec{v} k) = \nabla \cdot \left(\left[\mu + \frac{\mu_k}{\sigma_k} \right] \nabla k \right) + P - p\varepsilon \tag{12}$$

$$\frac{\partial \rho \varepsilon}{\partial t} + \nabla \cdot (\rho \vec{v} \varepsilon) = \nabla \cdot \left(\left[\mu + \frac{\mu_t}{\sigma_\varepsilon} \right] \nabla \varepsilon \right) + \frac{\varepsilon}{k} \left(C_{\varepsilon 1} P - C_{\varepsilon 2} p\varepsilon \right) \tag{13}$$

where P is the production rate of the ρk [4, 5]. Here, the default standard k-ε model constant values are implemented. In the turbulent flame case, the τ_{mix} term in Equation (5) is set as 0.1 [16].

3. LOCAL TIME STEPPING (LTS) SOLVER

The *reactingFoam* solver utilizes Pressure Implicit with Splitting of Operators (PISO) algorithm [23, 24] which needs to be stabilized by using a low maximum Courant–Friedrichs–Lewy (CFL) number, particularly in reacting flow cases [5, 11]. When a one-dimensional case is considered, the CFL number is defined as

$$CFL = \frac{v \Delta t}{\Delta x} \tag{14}$$

where v and Δx denote the local velocity and mesh size of the computational cell, respectively. Δt on the other hand, refers to the global time step. Referring to Equation (14), the global time step is adjusted at each iteration to fulfill the CFL condition and the same global time step is used for all the cells throughout the computational grid [25]. In this approach, the smallest cell with the highest velocity leads to the need of a small time step and consequently, the overall computational runtime becomes long. Although larger cells with lower velocity could be driven with much larger time steps, they were prohibited. The LTS version of the *reactingFoam* solver is used to run the simulations to steady state with an expedited calculation. The LTS approach is introduced to maximize the individual time step for each cell according to the local CFL number [26–28]. In the previous studies carried out by other authors, the LTS approach has been adopted to solve flow cases. In the present work, this concept is applied to solve reacting flow problem. The local time step limit is computed accounting for both the flow time scale, τ_{flow} and temperature source time scale, τ_{temp}. In the process of determining the flow time scale, a reciprocal of time step is calculated using Equation (15).

$$\frac{1}{\tau_{flow}} = \frac{\phi \cdot \sigma_s}{\max Co \cdot S_f \cdot \rho} \tag{15}$$

where ϕ is the mass flux and σ_s is the cell-to-cell distance. Besides this, *maxCo* denotes the maximum CFL number while S_f represents the surface magnitude. The reciprocal of temperature source time

scale as expressed by Equation (16) is dependent on the $\partial p/\partial t$ term and heat combustion due to combustion in the sensible enthalpy transport equation.

$$\frac{1}{\tau_{temp}} = \frac{\Delta t\left(\partial p / \partial t + \dot{\omega}_T\right)}{alphaTemp \cdot c_p \cdot T \cdot \rho} \tag{16}$$

alphaTemp is here designated to limit the change of the temperature per time step and hence to prevent instability in calculations. This parameter is particularly important for reacting flow simulations. Throughout the calculation, it is allowed to use a large time scale denoted by the parameter *maxDeltaT* in order to speed up the calculation. The solver then processes the time step fields by smoothing the variation in time step across the domain to avoid abrupt transitions caused by sudden changes in time step. This process is controlled by the smoothing coefficient, *rDeltaTSmoothingCoefficient*. Implementation of a *rDeltaTSmoothingCoefficient* value of unity does no smoothing, so each cell has its own time step fitting the *maxCo* number; while a unique time step is applied for the entire domain when the value is set to zero [26].

4. MESH CONFIGURATION AND BOUNDARY CONDITIONS

4.1 Mesh Configuration

Figure 1 depicts both the reflected 4-degree sector computational grids generated using the *blockMesh* utility in OpenFOAM software. The domain illustrated in Figure 1(a) is used to represent a section of the combustion chamber used for the DTU laminar premixed flame study [29] while the grid shown in Figure 1(b) is used for the Sandia Flame D simulation [30]. The temperature contour is used here for a better visualization of each boundary condition.

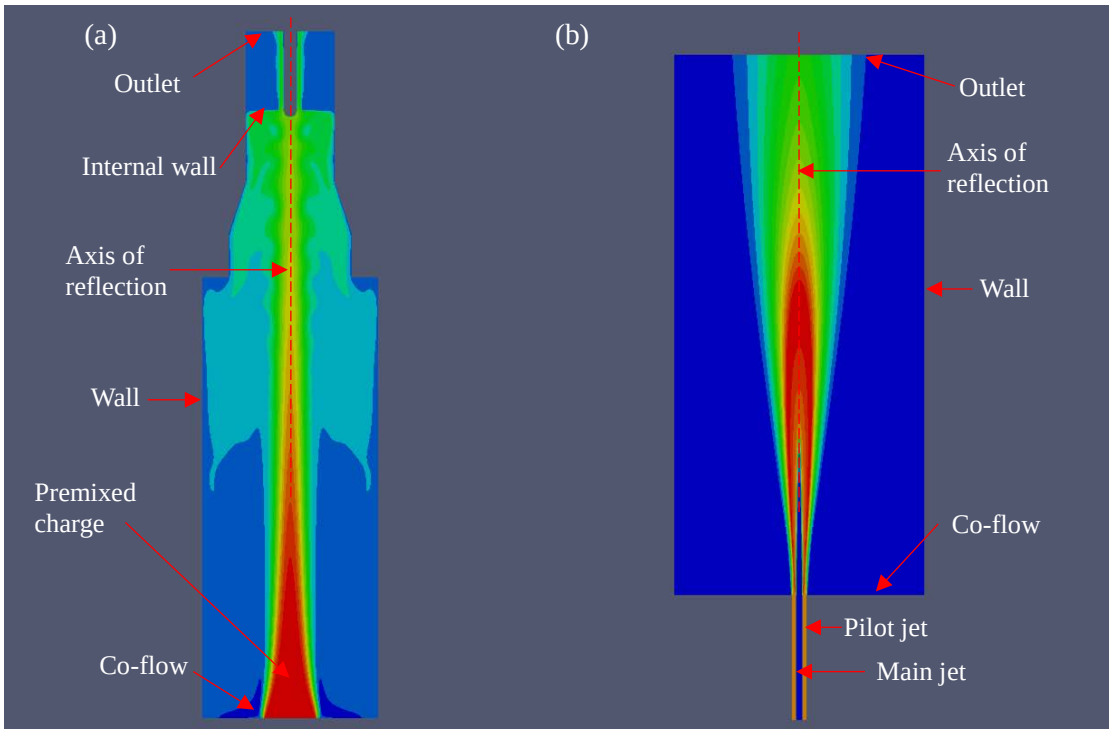

Figure 1. Reflected of the 2-D computational domains of the combustion chambers used for (a) DTU Helium-stabilized laminar premixed flame simulation and (b) Sandia Flame D simulation.

DTU helium-stabilized, laminar premixed flame

The experimental work of the laminar premixed flame was carried out by Ivarsson [29]. The work dealt with the post flame instability induced by the difference of gas densities at the downstream and upstream of the flame. The helium stabilization was developed based on the working principle of equalizing the gas densities by diluting the surrounding gas at the downstream of the flame with helium. The experimental setup was designed such that the premixed fuel/air charge entered the combustion chamber through the center inlet at a velocity of 0.135 m/s while the helium gas entered as a co-flow jet at a low velocity of 0.048 m/s. As illustrated in Figure 1(a), the combustion chamber also consists of an internal valve such that the helium gas can be trapped to stabilize the flame. A more detailed description of the experimental setup can be found in Ivarsson [29].

Based on the mesh sensitivity analysis, a fine mesh resolution is required at the regime above the premixed charge inlet in the flow direction in order to deal with the high species and temperature gradients along the combustion process. As such, the mesh size at the axial direction is set to 0.01 mm. The selection of 0.01 mm at the flame establishment area is verified by CHEMKIN's PREMIX code in which, the adaptive grid size is set to be smaller than 0.017 mm [29]. This mesh configuration is found sensitive to predict the change of laminar flame speed and hence the heat loss and flame temperature near the burner surface when the pre-exponential factor is varied. Otherwise, a coarser mesh size fails to capture the relocation of the flame even when the pre-exponential factor is increased. The mesh size at the exit next to the internal wall is set to 0.4 mm. A larger mesh was observed to induce fluctuation in the flow. In the regions where these gradients are less steep, the maximum axial and radial resolutions are allowed to reach 1.0 and 2.0 mm, respectively. The final computational grid consists of 113,527 hexahedron and 725 prima elements. Further refinement in the spatial resolution does not produce significant improvement in the accuracy of the predictions.

Sandia Flame D

The fuel was composed of 25% methane (CH_4) and 75% air by volume with a temperature of 294 K. The bulk velocity for the main fuel jet was 49.6 m/s. This corresponded to a Reynolds number of 22,400. Under this operating condition, only a small degree of local flame extinction was observed. Besides this, the surrounding pilot jet had an equivalent equilibrium composition to methane/air at mixture fraction of 0.27 with a temperature of 1880 K. The pilot jet velocity was set at 11.4 m/s. The third inlet was designated for the co-flowing air which its temperature was held at 291 K and entered the combustion chamber at a relatively low velocity of 0.9 m/s. All of the details regarding this flame are provided and regularly updated in the web site [30].

The mesh sensitivity analysis for the Sandia Flame D simulation shows that the axial spatial resolution influences the temperature prediction. Four different mesh sizes are examined and the maximum local temperature produced using a coarser mesh in the axial direction is found to be higher. The maximum local temperatures are 2446 K, 2356 K, 2302 K and 2295 K as the axial mesh size varies from 4.0, 2.0, 1.0 and 0.5 mm, respectively. It can be observed that the differences reduce with the mesh size. The mesh size of 1.0 mm is hence concluded to produce sufficiently mesh independence results. On the other hand, the spatial resolution in the radial direction has insignificant effects on temperature prediction. A fine resolution is however used here such that sufficient velocity data points are produced to compare against the experimental velocity profile. As such the radial mesh size is set as 0.2 mm and 0.25 at the main and pilot jet regions, respectively. The mesh size expands to 7.0 mm when it approaches the wall. The final computational grid consists of 72,000 hexahedron and 800 prima elements.

4.2 Boundary conditions

In both simulations, the fixed-value condition which is also known as Dirichlet boundary condition are enforced at the inlets for all variables except for pressure, that uses a Neumann boundary condition where the normal derivative i.e. gradient is zero. Nonslip walls are used, together with a

zero gradient for the other scalar variables, except for wall temperature that is set to a fixed value. The outlet is located at the top of the computational domain where ambient condition is used. For the outflow, Neumann boundary conditions are applied for all the scalar variables, except for pressure. The total pressure at the outlet is fixed at ambient pressure. Once the dynamic pressure varies accordingly to the velocity, the static pressure is recalculated to fulfill the designated total pressure. For the radiation modeling with P1-method, the Marshak's boundary condition is applied for all the inlets, outlet and walls.

In the Sandia Flame D case, the initial turbulent kinetic energy is defined using the turbulence intensity while the initial dissipation rate is defined by the associated mixing length. The hot mixture from the pilot jet ignites the fuel which is injected from the main jet. With such setup, the 'cold boundary condition' is not observed in the associated numerical simulation. The 'cold boundary condition' is however, a common problem in laminar premixed flame simulations [31]. In order to address this problem, the initial mixture temperature at premixed charge inlet is set at 1500 K such that it is sufficiently high to allow combustion to occur. The inlet temperature is then ramped down gradually over a specified period of time to the actual mixture temperature of 300 K. This is achieved by applying the time-varying boundary condition as depicted in Table 1. The timespan is selected such that the flame is well established and the combustion sustains by itself even the inlet temperature is low. All the boundary conditions implemented in the laminar premixed flame and turbulent non-premixed flame are summarized in Table 1 and Table 2, respectively.

Table 1. Boundary conditions implemented in the DTU helium-stabilized, laminar premixed flame simulation.

	Premixed charge	Helium co-flow	Wall	Outlet
P [Pa]	*zeroGradient*			*totalPressure*
T [K]	*timeVarying UniformFixedValue*	*fixedValue*		*zeroGradient*
v [m/s]	*fixedValue*			*fluxCorrected Velocity*
Y_i [-],Y_s [-],X_N [mol/kg]	*fixedValue*		*zeroGradient*	*inletOutlet*
G [kg/s^3]	*MarshakRadiation*			

Table 2. Boundary conditions implemented in the Sandia Flame D simulations.

	Main jet	Pilot jet	Co-flow	Wall	Outlet
P [Pa]	*zeroGradient*				*totalPressure*
T [K]	*fixedValue*				*zeroGradient*
v [m/s]	*fixedValue*				*fluxCorrected Velocity*
Y_i [-]	*fixedValue*				
k [m^2/s^2]	*turbulenceIntensityKineticEnergyInlet*			*kqRWallFunction*	*inletOutlet*
ε [m^2/s^3]	*turbulentMixingLengthDissipationRateInlet*			*epsilonWallFunction*	
G [kg/s^3]	*MarshakRadiation*				

5. RESULTS AND DISCUSSIONS

In the first part of this section, the convergence criterion is monitored to investigate if the *rareLTSFoam* produces steady-state solution. This is carried out using the laminar premixed flame test case. However, minor fluctuation at the downstream of the flame is observed in the experiment. Although it does not influence the optical measurement and investigation at the region of interest, it leads to residual oscillation in the simulations. As such, instead of the residuals, a physical property i.e. local temperature at the height of 150 mm is used as the convergence criterion [26]. The subsequent part of this section then discusses the effect of each LTS parameter on results accuracy, computational speed and calculation stability. It is then followed by the comparison of temperature/soot volume fraction profiles generated using the LTS solver against that recorded from the experiment for model validation purposes.

5.1 Convergence and performance benchmarking

Convergence

In this simulation of the rich laminar premixed flame, combustion, soot formation and radiation are taken into consideration. The associated PDE systems involved here are hence numerically stiff. Iteration-methods are usually exploited to run such simulation in a specified order to avoid a crash of the matrix-solver [2, 32]. Also, the iteration-method is necessary to ensure that the helium gas distribution is correct in the laminar premixed flame test case. Otherwise, the flow pattern becomes random and helium starts to distribute towards the wall instead of the flame. The helium gas hence fails to stabilize the flame and the flame starts to fluctuate again due to difference of densities at upstream and downstream of the flame. Likewise, an iteration-method is strategized for this simulation. The procedure used is as follows,

i) The simulation is initialized by setting a high temperature of 1500 K at the premixed charge inlet and gradually reducing the value to 300 K.
ii) Once the first steady-state solution is obtained, the associated field is mapped for initialization of other cases with different fuel compositions/chemical reactions.
iii) The radiation model is activated.
iv) The discretization for divergence is set to the scheme with second order accuracy.
v) The simulation is finalized by running with the PISO solver which is built by coupling the WSGGM and the Magnussen soot model with *reactingFoam*. The PISO solver is henceforth addressed as *rarePISOFoam*.

It is shown in Figure 2 that the solution remains steady state despite the laminar flame speed varies (indicated by the change of pre-exponential factor, *A*) as well as when the radiation model is activated. Also, there is no change in the temperature at the height of 150 mm by varying the discretization scheme to second order of accuracy. The flame fluctuation however, becomes more apparent at the height of above 260 mm. This in fact, replicates the experimental flame but it does not influence the analysis since the region of interest remains steady state. A further validation of the LTS solver is carried out by running the simulation using *rarePISOFoam*. The simulation is carried out for approximately 0.5s which is equivalent to 330,000 iterations and the solution remains steady-state.

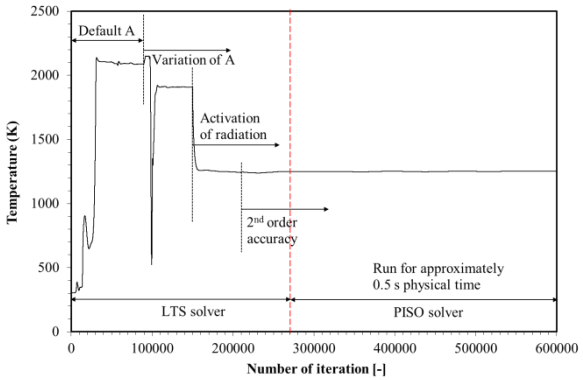

Figure 2. Plot of the convergence criterion of the simulation, the temperature at the height of 150 mm above the burner surface.

The LTS solver is found to provide an advantage in reducing computational runtime. As compared to the computational runtime consumed by the case ran fully with *rarePISOFoam* solver, a speedup of approximately fourteen-fold is obtained when the same *maxCo* number of 0.1 is used in both solvers. With such expedited calculation, the implementation of computational expensive fvDOM radiation model becomes more practical in the future work. Also, the evaluation of different, new radiation absorption/emission and soot formation/oxidation submodels can be carried out more efficiently.

Performance benchmarking of LTS parameters

The single-step ethylene (C_2H_4) reaction developed by Westbrook and Dryer [33] is used in the study. The performance benchmarking exercise shows that the *maxCo* number is the most significant factor to both stability and computational runtime among the four LTS parameter. A low CFL number of 0.1 is required in the beginning of the simulation (for approximately 20,000 iterations) such that the flame establishes at the region with fine resolution near the burner surface. The combusting flow is found to progress too rapidly and does not establish on top of the burner surface when a greater *maxCo* value is implemented. Higher *maxCo* values are allowed only after the fine-resolution region is filled with a well-established flame. Figure 3(a) demonstrates the convergence and result accuracy when different *maxCo* values are used. As observed, the simulation requires approximately 74,000 iterations for the mixture to fill up the entire computation domain. Result accuracy does not vary significantly when a higher *maxCo* number is implemented but much lesser number of iterations is required to obtain the steady state solution.

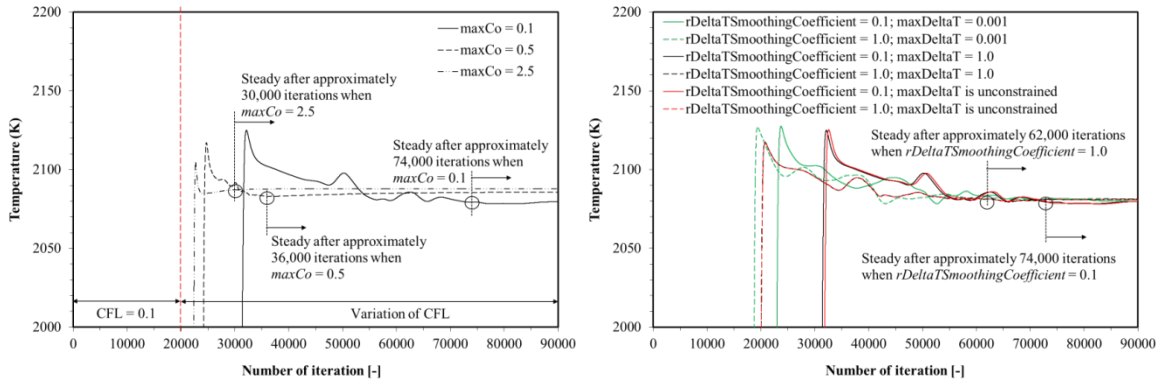

Figure 3. Plot of the convergence criterion of the simulation (a) when different *maxCo* values are used and (b) when different *rDeltaTSmoothingCoefficient* and *maxDeltaT* values are used.

Performance of the *rareLTSFoam* solver is further appraised by varying *alphaTemp*. Based on the study, the computational cost is found to be insensitive to *alphaTemp* i.e. the number of iterations required for convergence does not vary significantly. The system stability is however, dependent on this parameter. The calculation does not crash when the *alphaTemp* is increased from the baseline setup of 0.5% to 5%, 10% and 20 %. As *alphaTemp* value is raised to 50%, an impractical estimation of the local temperatures is observed and local temperatures in such case fall out of the temperature range given by the JANAF thermochemical table. Bearing in mind that the field mapping utility is commonly used in the simulation and the rate of change of the temperature is high when field mapping is exploited, a low *alphaTemp* value of 0.5 % is suggested to ensure the simulation stability.

An appraisal of *rDeltaTSmoothingCoefficient* parameter shown in Figure 3(b) reveals that this parameter is useful to reduce the number of iterations required for convergence. By increasing the coefficient value to unity, each cell has its own time step fitting the *maxCo* number and no smoothing is made. As such, the maximum overall time scale is raised and the solution converges earlier. The last investigated parameter is the *maxDeltaT*. Figure 3(b) illustrates that despite there is no constrain is set for the *maxDeltaT* value i.e. the time scale is allowed to rise unlimitedly, the overall maximum time scale is still prohibited by the *rDeltaTSmoothingCoefficient* to fulfill the condition given during the calculation. Hence, the maximum overall time scale is similar to that in the baseline setup if *rDeltaTSmoothingCoefficient* value is small and associated number of iterations to converge is not reduced. The unconstrained *maxDeltaT* has to be used together with a large number of *rDeltaTSmoothingCoefficient* so that the solution converges faster. It is hence concluded that *rDeltaTSmoothingCoefficient* is more influential to the computational cost here. Apart from these, both parameters are also found to be insensitive to the solution stability.

5.2 DTU helium-stabilized laminar premixed flame

Here, comparisons are made between the experimental measurement and simulated temperature profiles when differential radiation modeling approaches are used. The soot model implemented in OpenFOAM code is also evaluated by comparing the results to the soot volume recorded in the experiment. Ivarsson [29] in a separate work, has carried out a modeling of laminar premixed rich flame using the ANSYS CFX platform. The numerical results are adopted and exploited for validation of the current LTS solver. Here, the single-step ethylene (C_2H_4) reaction suggested by Ivarsson [29] as shown by Reaction (17) is implemented.

$$5C_2H_4^{0.1} + 7O_2^{1.65} = 3H_2O + CO_2 + 9CO + 7H_2 \qquad (17)$$

For the radiation modeling, the set of WSGGM coefficients used is based on Taylor and Foster et al. [19, 20]. Figure 4(a) depicts the experimental and simulated temperature generated by the *rareLTSFoam* solver and ANSYS CFX. Similar to the previous test case, the temperature along the axial direction remains rather uniform when radiation is not considered. An evaluation of WSGGM shows that the use of fitting coefficients for gas-phase radiation is insufficient to capture the radiative heat loss of the rich and sooty flame. The prediction is improved by substituting the submodel which soot radiation is considered. The radiative heat loss is more significant and associated temperature profile is closer to the experimental measurement. Also, the computed temperature profile using *rareLTSFoam* is comparable to that generated by ANSYS CFX [29], although the latter result is closer to measurement at the height of 0 to 90 mm. Yet, both the simulated results show steeper gradients i.e. the drop of temperature is greater. This could be attributed to the p_w/p_c ratio. The p_w/p_c ratio in the test case approximates 3 but the data set used here is meant for a ratio of 2. Further improvement is required by applying a more appropriate set of fitting coefficients for the radiation modeling of WSGGM. The temperature contours computed by OpenFOAM and ANSYS CFX coupled with soot radiation are demonstrated in Figure 5. As illustrated, the flame lift-off observed in the experiment is replicated. Replication of this feature is significant to produce the upstream temperature. Otherwise, the associated flame transports nearer to the cold burner surface. The heat loss due to convection is high and hence a predicted flame temperature near the burner surface is lower.

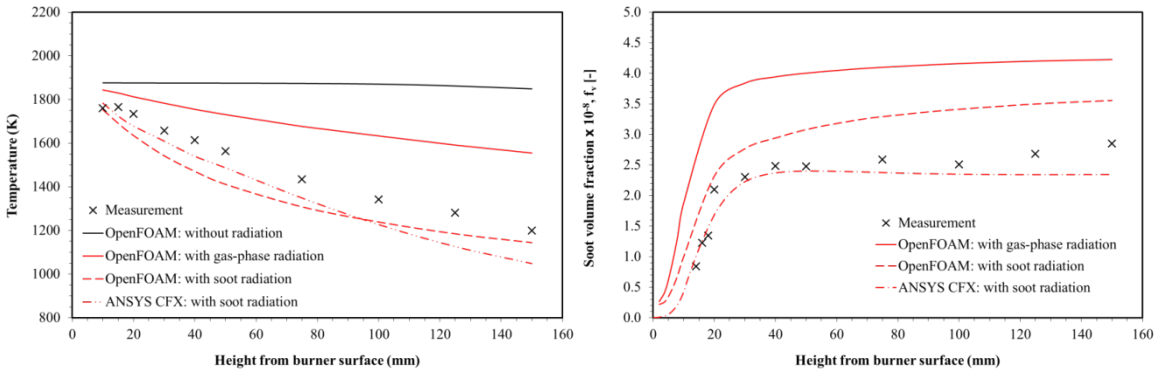

Figure 4. Comparisons of measured and simulated (a) temperature profiles and (b) soot volume fraction.

Figure 4(b) illustrates the comparison of measured and simulated soot volume fraction. The soot volume fraction calculated when the gas-phase radiation is used is much greater as compared to the measurement. This is attributed to the inaccurate associated temperature prediction. The overall soot volume fraction prediction is improved when the soot radiation is considered, particularly at the height of below 20 mm above the burner surface. It is however, overestimated when the height increases. A further improvement of both radiation and soot formation modeling is required and the Formulation of these models has to be carried out in parallel since these two phenomena are closely coupled.

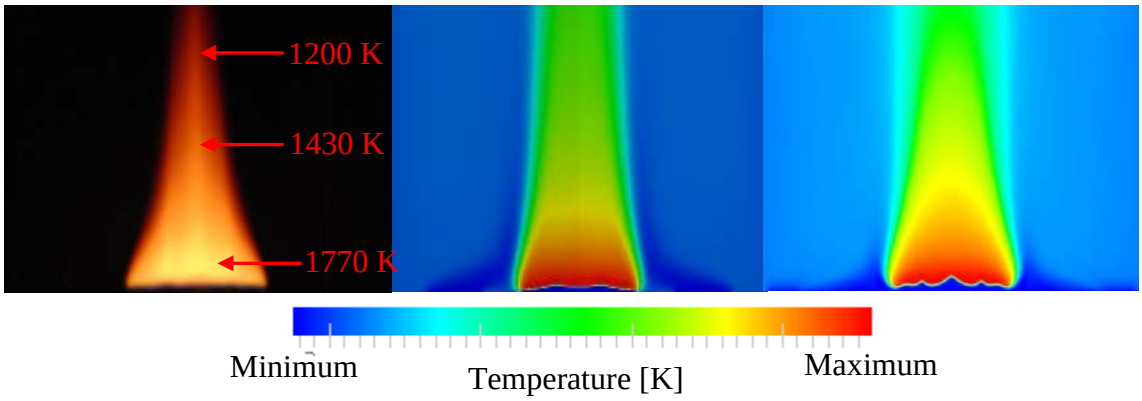

Figure 5. Comparisons of (a) flame images recorded from experiment against temperature contours [29] simulated by (b) OpenFOAM and (c) ANSYS CFX [29]. The minimum temperature is 300 K for both simulation cases while the maximum temperatures are 1836 K and 1810 K in the OpenFOAM and ANSYS CFX case, respectively.

5.3 Sandia Flame D

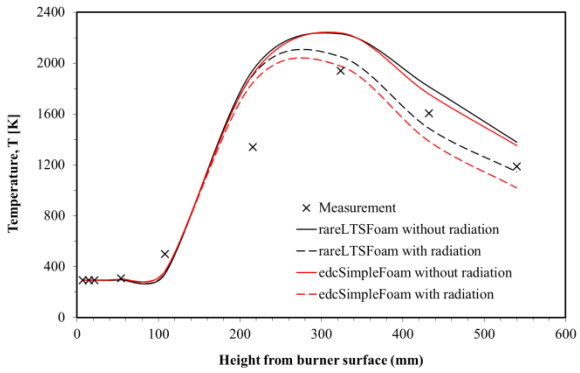

Figure 6. Comparisons of temperature profiles between experimental measurement and simulation results for the Sandia Flame D.

For a further model validation, *rareLTSFoam* is applied to simulate a more complex flame. Here, the model validation exploits the experimental data of the turbulent non-premixed Sandia Flame D data [30] which has been used to validate the *edcSimpleFoam* [1]. Akin to Christ's work, the single-step methane (CH_4) reaction proposed by Westbrook and Dryer as described by Reaction (18) is implemented here [33].

$$CH_4^{0.1} + 3O_2^{1.65} = 2H_2O + CO_2 \qquad (18)$$

For the radiation modeling, the WSGGM library which was published together with the *edcSimpleFoam* is directly adopted and integrated into *rareLTSFoam* and the set of WSGGM coefficients used is based on Smith et al. [18]. As depicted in Figure 6, the axial temperature profiles computed using both *rareLTSFoam* and *edcSimpleFoam* match the experimental measurement sufficiently well when the radiation modeling is activated. Also, it is observed that *rareLTSFoam* produces a closer temperature prediction at the upstream of the flame as compared to *edcSimpleFoam* results but *rareLTSFoam* requires higher number of iterations to reach steady-state solution. With both solvers, the simulated temperatures at the height of 200 to 300 mm are overestimated. This can be attributed to the implementation of the simplified, single-step global reaction. In the future work, a more detailed chemical kinetic mechanism will be applied together with the solvers for a better prediction of the combustion temperature.

6. CONCLUSIONS

The current work presents the development and validation of a LTS for the modeling of combustion and radiative heat transfer of two different flames. The new solver, *rareLTSFoam* is built based on the *LTSReactingParcelFoam*. WSGGM and Magnussen model are coupled with *rareLTSFoam* for the modeling of the radiative heat transfer and soot formation, respectively. The performance of each LTS parameter is also evaluated and the study reveals that *maxCo* is the most important factor in both calculation stability and computational cost. With the implementation of *rareLTSFoam* as well as their respective global reactions, temperature profiles in both laminar and turbulent flame test cases are replicated reasonably accurate at an expedited calculation. In the laminar premixed flame test case, a speedup of approximately fourteen-fold is obtained as compared to the computational runtime required by the counterpart, transient solver. The predicted temperature profile along the axial direction in the laminar flame case is comparable to that generated using the commercial CFD software, ANSYS CFX. A further improvement of both radiation and soot formation modeling is however, required in order to replicate the rich flame characteristics. Formulation of these models has to be carried out concurrently since these two phenomena are closely coupled. As compared to the performance of *edcSimpleFoam*, *rareLTSFoam* predicts temperature at the upstream of the flame but *rareLTSFoam* requires higher number of iterations to reach steady-state solution. This work shows that *rareLTSFoam* serves as a promising tool for the simulation of combustion, radiation and soot formation. Implementation of this solver reduces the computation runtime and therefore allows the use of computational expensive yet comprehensive radiation model such as fvDOM radiation model in the future work. At an expedited calculation, the evaluation of different, new radiation absorption/emission and soot formation/oxidation submodels is also facilitated.

REFERENCES

1. Christ D., “Simulating the combustion of gaseous fuels,” 6th OpenFoam Workshop Training Session, Pennsylvania, United States, 13-16 June, 2011.
2. Harasek M., Horváth A., Jordan C., Kuttner C., Maier C., Nagy J., Pohn S., Vienna University of Technology, “Steady state RANS simulations of a swirling, non-premixed industrial methane-air burner using edcSimpleFoam,” Available at <http://www.zid.tuwien.ac.at/fileadmin/files_zid/projekte/2011/11-166-2.pdf> [Accessed on 14 June 2012]
3. Andersen C., Nielsen N.E.L., “Numerical investigation of a BFR using OpenFOAM,” Aalborg University, Aalborg, 2008.
4. Kassem H.I., Saqr K.M., Aly H.S., Sies M.M., Wahlid M.A., “Implementation of the eddy dissipation model of turbulent non-premixed combustion in OpenFOAM,” International Commutation in Heat and Mass Transfer, 28 pp. 363-367, 2011.
5. Marzouk O. A., Huckaby E. D., “A comparative study of eight finite-rate chemistry kinetics for CO/H_2 combustion,” Engineering Applications of Computational Fluid Mechanics, 4, pp. 331-356, 2010.
6. Nogenmyr K.-J., Chan C., Duwig C., “Finite rate chemistry effects and combustor liner heat transfer studies in a framework of LES of turbulent flames-Investigation of pollutant formation using OpenFOAM,” 5th OpenFOAM Workshop, Gothenburg, Sweden, 2010.
7. Duwig C., Nogenmyr K.-J., Chan C., Dunn M.J., “Large Eddy Simulations of a piloted lean premixed jet flame using finite-rate chemistry,” Combustion Theory and Modelling, 15, pp. 537-568, 2011.
8. Duwig C., Ducruix S., Veynante D., “Studying the stabilization dynamics of swirling partially premixed flames by proper orthogonal decomposition,” Journal of Engineering of Gas Turbines and Power, 134, pp. 1-10, 2012.
9. Cuoci A., Frassoldati A., Faravelli T., Ranzi E., “Formation of soot and nitrogen oxides in unsteady counter flow diffusion flames,” Combustion and Flame, 156, pp. 2010-2022, 2009.
10. Cuoci A., Frassoldati A., Faravelli T., Ranzi E., “Kinetic modeling of soot formation in turbulent non-premixed flames,” Environmental Engineering Science, 25, pp. 1407-1422, 2008.

11.Messig D., Hunger F., Keller J., Hasse C., “Evaluation of radiation modeling approaches for non-premixed flamelets considering a laminar methane air flame,” Combustion and Flame, 160, pp. 251-264, 2013.
12.Anon, California Institute of Technology, Available at <http://www2.galcit.caltech.edu/EDL/public> [Accessed on 23 Nov 2012]
13.Wang L., Haworth D.C., Turns S.R., Modest M.F., “Interactions among soot, thermal radiation, and NO_x emissions in oxygen-enriched turbulent nonpremixed flames: A computational fluid dynamics modeling study,” Combustion and Flame, 141, pp. 170-179, 2005.
14.Modest F.M., second ed., “Radiative Heat Transfer,” Academic Press, California, 2003.
15.Magnussen B.F., Hjertager B.H., “On mathematical modeling of turbulent combustion with special emphasis on soot formation and combustion,” Symposium (International) on Combustion, 16, pp. 719-729, 1977.
16.Chomiak J., Karlsson A., “Flame liftoff in diesel sprays,” Proceedings of the Combustion Institute, 26, pp. 2557-2564, 1996.
17.Vdovin A., “Radiation heat transfer in OpenFOAM,” Chalmers University of Technology, Available at <http://www.tfd.chalmers.se/~hani/kurser/OS_CFD_2009/AlexeyVdovin/Radiation_in_OpenFoam_final.pdf> [Accessed on 20 August 2012]
18.Smith T.F., Shen Z.F., Friedman J.N., “Evaluation of Coefficients for the Weighted Sum of Gray Gases Model,” Journal of Heat Transfer, 104, pp. 602-608, 1982.
19.Taylor P.B., Foster P.J., “The total emissivities of luminous and non-luminous flames,” International Journal of Heat and Mass Transfer, 17, pp. 1591-1605, 1974.
20.Taylor P.B., Foster P.J., “Some gray gas weighting coefficients for CO_2-H_2O-soot mixtures,” International Journal of Heat and Mass Transfer, 18, 1331-1332, 1975.
21.Tesner P.A., Smegiriova T.D., Knorre V.G, “Kinetics of dispersed carbon formation,” Combustion and Flame, 17, pp. 253-260, 1971.
22.Versteeg H.K., Malalasekera W., “An introduction to computational fluid dynamics: The finite volume method,” Second Ed., Pearson Education Limited, England, 2007.
23.Issa R.I., “Solution of the implicitly discretised fluid flow equations by operator-splitting,” Journal of Computational Physics, 62, pp. 40-65, 1985.
24.Oliveira P.J., Issa R.I., “An improved PISO algorithm for the computation of buoyancy-driven flows,” Numerical Heat Transfer Part B, 40, pp. 473-493, 2001.
25.Courant R., Friedrichs K., Lewy H., “On the partial difference equations of mathematical physics,” IBM Journal of Research and Development, 11, pp. 215-234, 1967.
26.Becker M., “dhcaeLTSThermoParcelSolver,” DHCAE Tools, Available at <http://www.dhcae-tools.com/images/dhcaeLTSThermoParcelSolver.pdf> [Accessed on 19 July 2012]
27.Anon, “OpenFOAM The Foundation,” Available at <http://www.openfoam.org/version2.0.0/steady-vof.php> [Accessed on 17 March 2012]
28.Arnone A., Liou M.-S., Povinelli L.A., “Multigrid time-accurate integration of Navier Stokes equations,” NASA Technical Memorandum 106373 ICOMP-93-97, Lewis Research Center, Cleveland, Ohio and University of Florence, Florence, Italy November 1993.
29.Ivarsson A., “Modeling of heat release and emissions from droplet combustion of multi component fuels in compression ignition engines,” PhD thesis, Technical University of Denmark, Lyngby, 2009.
30.Barlow, R., Frank, J., “Piloted CH_4/air flames C, D, E, and F – Release 2.1,” Sandia National Laboratories, Available at http://www.sandia.gov/TNF/DataArch/FlameD/SandiaPilotDoc21.pdf. [Accessed on 5 September 2012]
31.Poinsot T.J., Veynante D., “Theoretical and Numerical Combustion,” Third Ed., Aquaprint, Bordeaux, 2001.
32.Frassoldati A., Frigerio S., Colombo E., Inzoli F., Faravelli T., “Determination of NO_x emissions from strong swirling confined flames with an integrated CFD-based procedure,” Chemical Engineering Science, 60, 2851-2869, 2005.
33.Westbrook C.K., Dryer F.L., “Simplified reaction mechanism for the oxidation of hydrocarbon fuels in flames,” Combustion Science and Technology, 27, pp. 31-43, 1981.